

**This is a self-archived version of an original article. This version may differ from the original in pagination and typographic details.**

**Author(s):** Kim, Yongbin; Morozov, Dmitry; Stadnytskyi, Valentyn; Savikhin, Sergei; Slipchenko, Lyudmila

**Title:** Predictive First-principles Modeling of a Photosynthetic Antenna Protein : The Fenna-Matthews-Olson Complex

**Year:** 2020

**Version:** Accepted version (Final draft)

**Copyright:** © 2020 American Chemical Society

**Rights:** In Copyright

**Rights url:** <http://rightsstatements.org/page/InC/1.0/?language=en>

**Please cite the original version:**

Kim, Y., Morozov, D., Stadnytskyi, V., Savikhin, S., & Slipchenko, L. (2020). Predictive First-principles Modeling of a Photosynthetic Antenna Protein : The Fenna-Matthews-Olson Complex. *Journal of Physical Chemistry Letters*, 11(5), 1636-1643.  
<https://doi.org/10.1021/acs.jpcllett.9b03486>

Physical Insights into Light Interacting with Matter

**Predictive First-principles Modeling of a Photosynthetic  
Antenna Protein: The Fenna-Matthews-Olson Complex**

Yongbin Kim, Dmitry Morozov, Valentyn Stadnytskyi, Sergei Savikhin, and Lyudmila Slipchenko

*J. Phys. Chem. Lett.*, **Just Accepted Manuscript** • DOI: 10.1021/acs.jpcllett.9b03486 • Publication Date (Web): 04 Feb 2020

Downloaded from [pubs.acs.org](https://pubs.acs.org) on February 5, 2020

**Just Accepted**

“Just Accepted” manuscripts have been peer-reviewed and accepted for publication. They are posted online prior to technical editing, formatting for publication and author proofing. The American Chemical Society provides “Just Accepted” as a service to the research community to expedite the dissemination of scientific material as soon as possible after acceptance. “Just Accepted” manuscripts appear in full in PDF format accompanied by an HTML abstract. “Just Accepted” manuscripts have been fully peer reviewed, but should not be considered the official version of record. They are citable by the Digital Object Identifier (DOI®). “Just Accepted” is an optional service offered to authors. Therefore, the “Just Accepted” Web site may not include all articles that will be published in the journal. After a manuscript is technically edited and formatted, it will be removed from the “Just Accepted” Web site and published as an ASAP article. Note that technical editing may introduce minor changes to the manuscript text and/or graphics which could affect content, and all legal disclaimers and ethical guidelines that apply to the journal pertain. ACS cannot be held responsible for errors or consequences arising from the use of information contained in these “Just Accepted” manuscripts.

1  
2  
3  
4  
5  
6  
7 Predictive First-Principles Modeling of a  
8  
9  
10  
11 Photosynthetic Antenna Protein:  
12  
13  
14  
15 The Fenna-Matthews-Olson Complex  
16  
17  
18  
19

20 *Yongbin Kim<sup>a</sup>, Dmitry Morozov<sup>b</sup>, Valentyn Stadnytskyi<sup>c,d</sup>, Sergei Savikhin<sup>c</sup>, and Lyudmila V.*  
21 *Slipchenko<sup>a\*</sup>*  
22  
23  
24  
25  
26  
27  
28

29 <sup>a</sup> Department of Chemistry, Purdue University, 560 Oval Drive, West Lafayette, IN 47907  
30  
31

32 <sup>b</sup> Nanoscience Center and Department of Chemistry, University of Jyväskylä, P.O. Box 35, 40014,  
33  
34 Finland  
35  
36

37 <sup>c</sup> Department of Physics and Astronomy, Purdue University, 525 Northwestern Avenue, West  
38  
39 Lafayette, IN 47907  
40  
41  
42

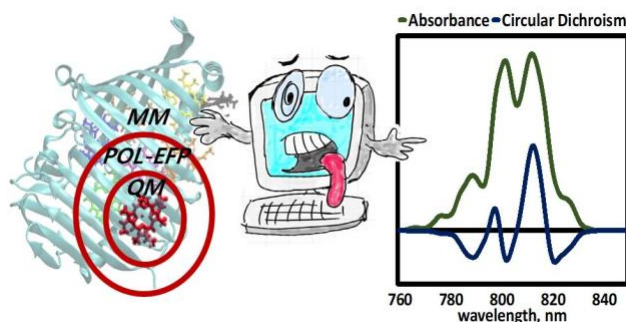
43 <sup>d</sup> Laboratory of Chemical Physics, National Institute of Diabetes, Digestion and Kidney Diseases,  
44  
45 National Institutes of Health, 5 Memorial Drive, Bethesda, MD  
46  
47  
48  
49  
50

51  
52 **Corresponding Author**  
53

54 \*Lyudmila V. Slipchenko; email: lslipchenko@purdue.edu  
55  
56  
57  
58  
59  
60

1  
2  
3  
4  
5  
6  
7 **ABSTRACT** High efficiency of light harvesting in photosynthetic pigment-protein complexes  
8  
9 is governed by evolutionary-perfected protein-assisted tuning of individual pigment properties and  
10  
11 inter-pigment interactions. Due to the large number of spectrally overlapping pigments in a  
12  
13 typical photosynthetic complex, experimental methods often fail to unambiguously identify  
14  
15 individual chromophore properties. Here we report a first principles-based modeling protocol  
16  
17 capable of predicting properties of pigments in protein environment to a high precision. The  
18  
19 technique was applied to successfully uncover electronic properties of the Fenna-Matthews-Olson  
20  
21 (FMO) pigment-protein complex. Each of the three subunits of the FMO complex contains eight  
22  
23 strongly coupled bacteriochlorophyll *a* (BChl *a*) pigments. The excitonic structure of FMO can be  
24  
25 described by an electronic Hamiltonian containing excitation (site) energies of BChl *a* pigments  
26  
27 and electronic couplings between them. Several such Hamiltonians have been developed in the  
28  
29 past based on the information from various spectroscopic measurements of FMO; however, fine  
30  
31 details of the excitonic structure and energy transfer in FMO, especially assignments of short-lived  
32  
33 high-energy sites, remain elusive. Utilizing polarizable embedding QM/MM with the effective  
34  
35 fragment potentials (EFP) we were able to compute the electronic Hamiltonian of FMO that is in  
36  
37 general agreement with previously reported empirical Hamiltonians and quantitatively reproduces  
38  
39 experimental absorption and circular dichroism (CD) spectra of the FMO protein. The developed  
40  
41 computational protocol is sufficiently simple and can be utilized for predictive modeling of other  
42  
43 wild type and mutated photosynthetic pigment-protein complexes.  
44  
45  
46  
47  
48  
49  
50  
51  
52  
53  
54  
55  
56  
57  
58  
59  
60

## TOC GRAPHICS



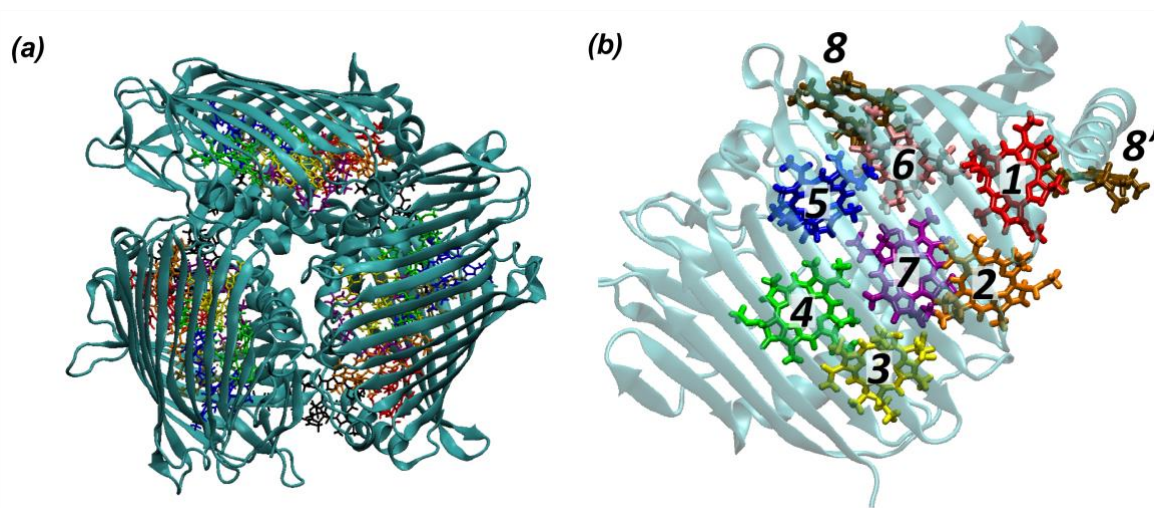
## KEYWORDS

pigment-protein complex, Fenna-Matthews-Olson protein, QM/MM, QM/EFP, effective fragment potential, polarizable embedding

Plants, algae and photosynthetic bacteria capture solar radiation by means of pigment-protein antenna complexes. A variety of natural antenna complexes evolved to maximize photosynthetic efficiency in different environments. The light harvesting and energy transfer efficiency of these complexes approaches 100% and is governed by electronic properties of individual light-absorbing pigments as well as by couplings between the pigments. While molecular structures of many antenna complexes have been determined by x-ray diffraction, the information about electronic energy levels and energy transfer dynamics often lacks desired precision as it is

1  
2  
3 primarily deduced from optical data. Most of the antenna complexes contain large number of  
4 pigments (up to ~250,000 in chlorosome antenna<sub>1</sub>) with overlapping optical spectra leading to  
5 spectral congestion that precludes unambiguous identification of properties of individual  
6 pigments and, as a result, multiple models can be proposed to fit the same data.  
7  
8  
9  
10  
11

12  
13 The Fenna-Matthews-Olson (FMO) pigment-protein complex, found in green sulfur bacteria,  
14 is one of the most thoroughly studied photosynthetic proteins (see Figure 1).<sup>2-37</sup> The primary  
15 function of FMO is to transfer the excitation energy from a much larger chlorosome antenna to  
16 the intramembrane reaction center complex, where electronic excitation initiates charge transfer  
17 process.  
18  
19  
20  
21  
22  
23  
24  
25



44  
45  
46  
47  
48  
49

**Figure 1.** (a) FMO trimer of the *Chlorobaculum Tepidum*, (b) FMO monomer with BChl *a* pigments.

50  
51  
52  
53  
54  
55  
56  
57  
58  
59  
60

The FMO complex is a trimer possessing  $C_3$  symmetry. Each subunit encloses seven bacteriochlorophyll *a* (BChl *a*) chromophores and binds the eighth BChl *a* pigment between the subunits. Close packing of BChl *a* pigments in each monomer subunit leads to strong excitonic

1  
2  
3 interactions and delocalization of excited states over multiple pigments. A relative structural  
4 simplicity combined with intricate excitonic structure makes the FMO complex a favorite object  
5  
6 for developing and testing new computational and experimental techniques. For example, FMO  
7  
8 was the first pigment-protein complex, for which quantum coherences and beatings between  
9  
10 excitonic states were observed by Savikhin *et al* in 1997.<sup>38</sup> The study of excitonic structure and  
11  
12 coherence in this complex led later to the development of a two-dimensional spectroscopy <sup>8, 39-41</sup>.  
13  
14 To model excitonic interactions and energy transfer in FMO, a number of different electronic  
15  
16 Hamiltonians have been proposed<sup>6, 8, 10, 12, 14, 18-19, 23, 25</sup>, most of which were obtained by a  
17  
18 combination of structural data and fits to available experimental measurements. While the off-  
19  
20 diagonal elements of a Hamiltonian represent electronic couplings between pigments and can be  
21  
22 estimated using dipole-dipole approximation from available x-ray structures, the diagonal  
23  
24 energies (individual transition energies) cannot be observed directly in experiment and are  
25  
26 inferred from fits to spectroscopic data. This approach results in a significant ambiguity in  
27  
28 determination of BChl *a* site energies and typically does not account for environment-driven  
29  
30 variations in transition dipole moments of individual pigments and inter-pigment couplings.  
31  
32 While molecular modeling based on structural data could provide unambiguous assignment of  
33  
34 excitonic interactions and energy flow in FMO, internal complexity of the system and necessity  
35  
36 to sample protein degrees of freedom, accurately describe electronic structure and couplings  
37  
38 between BChl pigments, and vibronic interactions between pigments and the protein  
39  
40 environment, makes this task challenging. <sup>10, 15, 19-24, 26-27, 29, 35, 42-44</sup>

41  
42 In this contribution, we report a multi-scale first-principles modeling that accurately  
43  
44 reproduces the absorption and circular dichroism (CD) spectra of the FMO complex based solely  
45  
46 on its x-ray structure and uses no other input from experiments. We show that a quantum  
47  
48  
49  
50  
51  
52  
53  
54  
55  
56  
57  
58  
59  
60

1  
2  
3 mechanical description of internal structures of BChl *a* pigments and embedding of pigments in a  
4 polarizable protein environment are the leading factors that provide excitonic structure consistent  
5 with experimental absorption and CD spectra. The developed protocol can be readily applied to  
6 other pigment-protein complexes with computational time scaling linearly with the number of  
7 antenna pigments.  
8  
9

10  
11  
12  
13  
14  
15  
16 The computational protocol, described in detail in Supporting Information, consisted of three  
17 main steps. First, the structure of the FMO trimeric complex from *Chlorobaculum tepidum*,  
18 formerly known as *Chlorobium tepidum*, (PDB ID: 3ENI) was protonated, immersed in water  
19 solvent, and equilibrated in a series of molecular dynamics (MD) simulations at ambient  
20 conditions with Amber03 classical force field. 100 configurations were extracted from the last 30  
21 ns of the equilibrated MD trajectory, shown in Figure S1. Second, constrained quantum  
22 mechanics / molecular mechanics (QM/MM) geometry optimizations, with QM regions  
23 containing one BChl *a* pigment and few strongly-interacting amino acids (AA) including the  
24 Mg-coordinating AA, were performed for each BChl *a* at each of the 100 selected  
25 configurations. Only the QM regions described with PBE0/6-31G(d) and shown in Figure S2 of  
26 Supporting Information were subject to geometry optimizations, thus removing inaccuracies  
27 caused by a classical force field description of the chromophore pocket. Finally, excited state  
28 calculations were performed at each structure with electrostatic embedding QM/MM and  
29 polarizable embedding QM/EFP model (EFP - effective fragment potential) models. The extent  
30 of the quantum and classical regions for each BChl *a* is outlined in Supporting Information  
31 (Figures S5 and S6); time-dependent density functional theory (TD-DFT) PBE0/6-31G(d) was  
32 used to describe electronic excitations. These calculations produced excitation site energies and  
33  
34  
35  
36  
37  
38  
39  
40  
41  
42  
43  
44  
45  
46  
47  
48  
49  
50  
51  
52  
53  
54  
55  
56  
57  
58  
59  
60



1  
2  
3 transition charges for each BChl *a*; the latter were used to compute electronic couplings between  
4  
5 pigments.  
6

7  
8  
9 In the described computational procedure, two steps critically affect the quality of results, as  
10  
11 we demonstrate below. These are (i) QM/MM geometry optimizations with sufficiently large  
12  
13 QM regions, and (ii) excited state calculations in a polarizable protein environment. As shown in  
14  
15 Figure 2a, the electronic excitation energies of BChl *a* pigments (without inclusion of protein  
16  
17 environment, aka “gas phase” site energies) with structures extracted directly from the MD  
18  
19 trajectory snapshots are essentially indistinguishable between each other due to large fluctuations  
20  
21 of BChl *a* internal structures during molecular dynamics and general limitations of the classical  
22  
23 force field. On the other hand, gas-phase site energies computed at the QM/MM optimized  
24  
25 structures fluctuate much less, such that energy differences between different sites become more  
26  
27 pronounced. The differences in gas-phase site energies originate in geometrical constraints  
28  
29 imposed by the protein scaffold on each BChl *a* pigment. Comparison of site energies computed  
30  
31 at the MM-optimized and QM/MM optimized structures, shown in Fig. S7 of SI, further  
32  
33 demonstrates importance of correcting the BChl *a* structures at the QM level.  
34  
35  
36  
37  
38

39  
40 We also found that inclusion of several neighboring AAs in the QM regions significantly  
41  
42 influenced the BChl *a* internal structures during the QM/MM geometry optimizations. The  
43  
44 guideline for selecting these “critical” AAs came from considering effects of individual AAs on  
45  
46 BChl *a* excitation energies, i.e, solvatochromic shifts due to individual neighboring AAs. Details  
47  
48 of that procedure are discussed in Supporting Information.  
49  
50

51  
52 The second critical step in our computational protocol is employing polarizable QM/EFP  
53  
54 model<sup>45-51</sup> for describing excitation energies of BChl *a* chromophores. The EFP method is a  
55  
56  
57  
58  
59  
60

1  
2  
3 model potential providing a rigorous description of intermolecular interactions from first  
4 principles.<sup>49, 52-59</sup> The EFP method treats a molecular system as a collection of rigid EFP  
5 fragments, interactions among which are described as a sum of Coulomb, polarization,  
6 dispersion, and exchange-repulsion terms. QM/EFP model, i.e. coupling of EFP subsystem to an  
7 *ab-initio* region, can be classified as a polarizable embedding QM/MM approach in which  
8 effective fragments interact with the QM region via electrostatic and polarization one-electron  
9 operators.<sup>47, 51-52, 60</sup> Therefore, charge distribution on EFP fragments is able to respond self-  
10 consistently to electron density fluctuations of the QM region.<sup>47-48</sup> Electrostatic potential of EFP  
11 fragments is modeled using multipoles up to octupoles centered at atoms and bond-mid-points;  
12 polarization potential is modeled using induced dipoles created as a response of distributed  
13 anisotropic polarizabilities to the electric field due to surrounding fragments and QM region.  
14 Distributed multipoles and polarizabilities are pre-computed for each unique fragment and stored  
15 as fragment parameters. A peptide chain is split into individual AA fragments along C-C bonds,  
16 as described in Ref. 50 and Supporting Information.

17  
18  
19 To demonstrate the importance of polarizable embedding in description of excitation energies  
20 in the FMO complex, we compare the site energies (averaged over 100 snapshots) computed  
21 with electrostatic embedding models QM/MM and QM/EFP-noPOL and with polarizable  
22 embedding QM/EFP (see Figure 2b). Partial charges (Amber03, the same as in classical MD  
23 simulations) were used to represent the environment in QM/MM model, while distributed  
24 multipoles up to octupoles centered on atoms and bond mid-points were used in QM/EFP-  
25 noPOL model. QM/EFP utilizes both distributed multipoles and polarizabilities to account for  
26 self-consistent polarization of the QM region and its environment. As Figure 2b demonstrates,  
27 the QM/EFP-noPOL and QM/MM schemes produce similar average site energies implying that

the inclusion of higher electrostatic multipoles in the description of electronic densities of AAs does not contribute significantly to solvatochromic shifts of BChl *a* pigments in the FMO complex. Noteworthy, both electrostatic embedding models do not differentiate well between different sites, producing similar solvatochromic shifts of 70-130  $\text{cm}^{-1}$  for sites #1, #3, #4, #5, #6, and #7 (110-130  $\text{cm}^{-1}$  shifts for sites #4, #5, #6, #7). In contrast to the electrostatic embedding models, the polarizable embedding QM/EFP results in distinct site energies and dramatically stabilizes excitation energy of site #3, which has been proposed to be an exit site of the FMO complex.<sup>5-6, 8, 15-16, 19, 23, 25</sup>

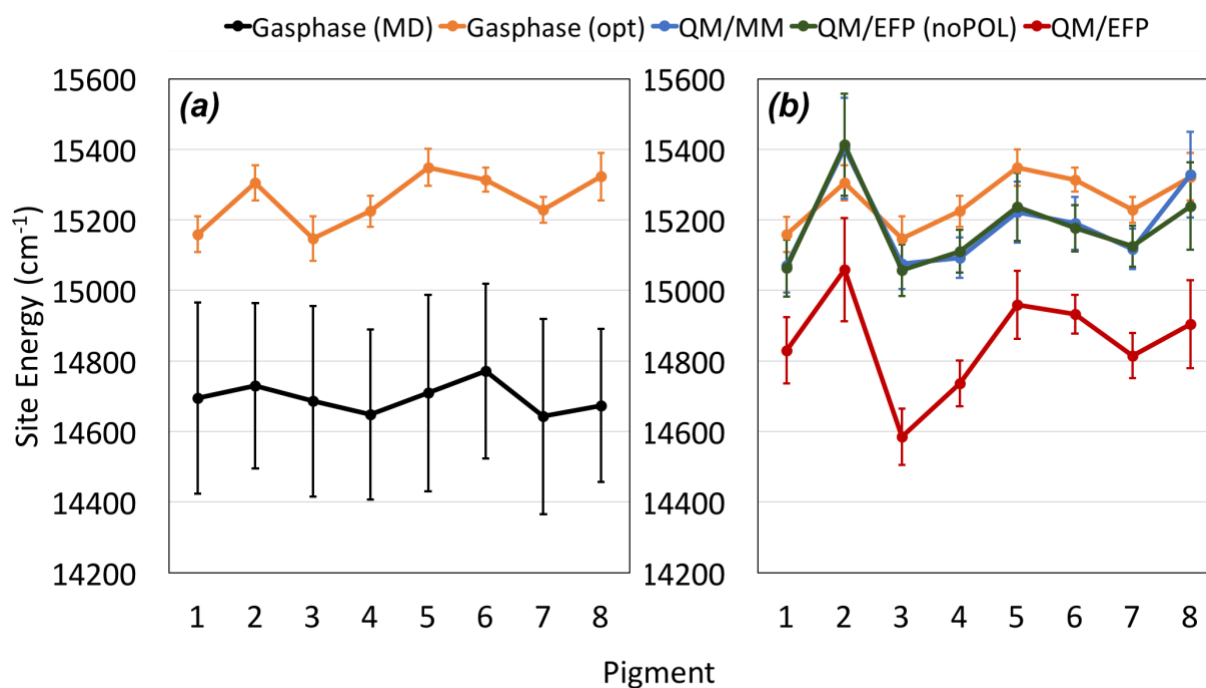


**Figure 2.** BChl *a* site energies averaged over 100 structures with standard deviations shown as vertical error bars. (a) Gas-phase (without protein environment) site energies computed for structures directly extracted from MD snapshots (black) and after QM/MM geometry optimizations (orange). (b) Gas phase (orange), QM/MM (blue), QM/EFP-noPOL (green) and QM/EFP (red) site energies computed for structures after QM/MM geometry optimizations.

1  
2  
3 Fluctuations of the QM/EFP site energies, originating in thermal motion of a protein scaffold  
4 captured by sampling of 100 protein structures, are visualized in Figure 3. Figure 3 also  
5  
6 compares the average values of the QM/EFP site energies (shown with black vertical lines) with  
7  
8 the excitation energies utilized in empirical Hamiltonians by Kell and Brixner (shown with blue  
9  
10 and red arrows, respectively).<sup>8, 25</sup> For an easier comparison with empirical Hamiltonians and  
11  
12 experimental spectra, QM/EFP site energies are shifted by  $-2430\text{ cm}^{-1}$  and QM/MM and  
13  
14 QM/EFP-noPOL site energies are shifted by  $-2800\text{ cm}^{-1}$ . A mismatch between absolute values of  
15  
16 experimental and computed excitation energies of BChls originates in well-known intrinsic  
17  
18 inaccuracies of a chosen level of theory (PBE0 functional in 6-31G\* basis set).<sup>61-62</sup> However, it  
19  
20 is expected that the chosen level of theory reasonably describes a potential energy surface of the  
21  
22 excited state (i.e., relative energy changes due to vibrational motion of a chromophore), and  
23  
24 relative energy changes due to interaction of the excited state with the protein environment. It is  
25  
26 these relative energy changes (due to slight geometrical distortions and interactions with the  
27  
28 heterogeneous protein environment) that determine energetic order of site energies and shapes of  
29  
30 the absorption and CD spectra.

31  
32  
33 As seen in Figure 3, there is a remarkable agreement between the average site energies from  
34  
35 the QM/EFP model and Kell's and Brixner's Hamiltonians for the three lowest sites #1, #3, #4,  
36  
37 and #7, while the energies of higher-energy sites deviate from each other. The deviations  
38  
39 between empirical model Hamiltonians for high-energy sites are not surprising as it is harder to  
40  
41 unambiguously deduce these energies from experiment due to short lifetimes and broader  
42  
43 spectral bandwidth of high-energy states. On the other hand, the accuracy of the QM/EFP site  
44  
45 energies is expected to be similar for all sites.

1  
2  
3 As follows from Figure 3, widths of energy distributions of sites #3, #4, #6, and #7 are  
4  
5 comparable to each other. In general, bacteriochlorin heads of these sites have at least one H-  
6  
7 bond with neighboring AAs in addition to coordination with N atoms of histidine (HIS) residues  
8  
9 (see Figure S2 in Supporting Information). On the contrary, sites #1, #5 and #8 do not have H-  
10  
11 bonds to nearby AAs and are somewhat weaker bound to the protein scaffold. As a consequence,  
12  
13 the excitation energy distribution of site #5 is wider than that of BChls that are H-bonded to a  
14  
15 protein. Additionally, as site #8 is not fully embedded in a protein envelope, its motion is even  
16  
17 less constrained, resulting in a significantly larger spread of excitation energies. In the case of  
18  
19 site #2 that also shows a very large spread of energies, Mg is coordinated by a water molecule  
20  
21 that moves freely in MD simulations such that BChl *a* #2 is found four-coordinated in about half  
22  
23 of the snapshots. Additionally, several other water molecules that are present in a cavity near the  
24  
25 BChl *a* #2 head-group change their positions and H-bonding patterns during MD simulations and  
26  
27 produce significant fluctuations to the site energy. Hence, we conclude that the width of the site  
28  
29 energy distribution is largely governed by the effective H-bonding of BChl *a* heads with the  
30  
31 protein scaffold as well as fluctuations of Mg-coordinating residues.  
32  
33  
34  
35  
36  
37

38  
39 As a side note, analysis of excitation energies computed at 100 protein structures does not  
40  
41 show any statistically significant correlation in fluctuations of site energies of different pigments,  
42  
43 which agrees with previous discussion of this subject in literature.<sup>15, 29</sup>  
44  
45

46  
47 Electronic couplings were computed using transition charges TrEsp of each pigment obtained  
48  
49 by a fit to a transition density with a constraint preserving the value of the transition dipole  
50  
51 moment (TDM). Further, for computing electronic couplings, transition dipoles and  
52  
53 corresponding transition charges were scaled to match (on average) experimental TDM of BChl  
54  
55 *a*, as explained in detail in SI. No additional environment-induced screenings were utilized in  
56  
57  
58  
59  
60

1  
2  
3 coupling calculations. Influence of polarizable environment on the electronic couplings in  
4 photosynthetic complexes was explored previously and found to be nonnegligible<sup>42, 63-64</sup>;  
5  
6 however, we leave a detailed analysis of these effects to future work.  
7  
8  
9

10  
11 Combining site energies with electronic couplings between different pairs of BChls, computed  
12 using transition charges TrEsp as explained in detail in Supporting Information, results in an  
13 electronic Hamiltonian that determines excitonic interactions in the FMO complex. The thermal  
14 motion of the protein produces fluctuations both of site energies and electronic couplings, such  
15 that each structural snapshot produces a unique Hamiltonian. Figure 4 provides an averaged  
16 QM/EFP Hamiltonian in which each matrix element is computed as an average of the  
17 corresponding matrix elements from 100 structures. Standard deviations of all Hamiltonian  
18 matrix elements are also shown in Figure 4. Analogous average QM/MM and QM/EFP-noPOL  
19 Hamiltonians are reported in Figure S9 of Supporting Information. Note that these Hamiltonians  
20 include BChl *a* #8' that is the closest to BChl *a* #1 (see Figure 1). While BChl *a* #8' formally  
21 belongs to a different protein subunit, it interacts stronger with the pigments in this subunit than  
22 BChl *a* #8 that is positioned further away and has negligible interactions with pigments of the  
23 same unit. Inspection of the average Hamiltonian in Figure 4 shows that the couplings are the  
24 strongest between neighboring pigments, i.e. in pairs #1-#2, #2-#3, etc., which agrees with  
25 empirical Hamiltonians. Additionally, central BChl *a* #7 interacts strongly with sites #3 and #4.  
26 Significant fluctuations in couplings are observed in pairs #5-#6, #3-#4 and #3-#7.  
27  
28  
29  
30  
31  
32  
33  
34  
35  
36  
37  
38  
39  
40  
41  
42  
43  
44  
45  
46  
47  
48  
49  
50  
51  
52  
53  
54  
55  
56  
57  
58  
59  
60

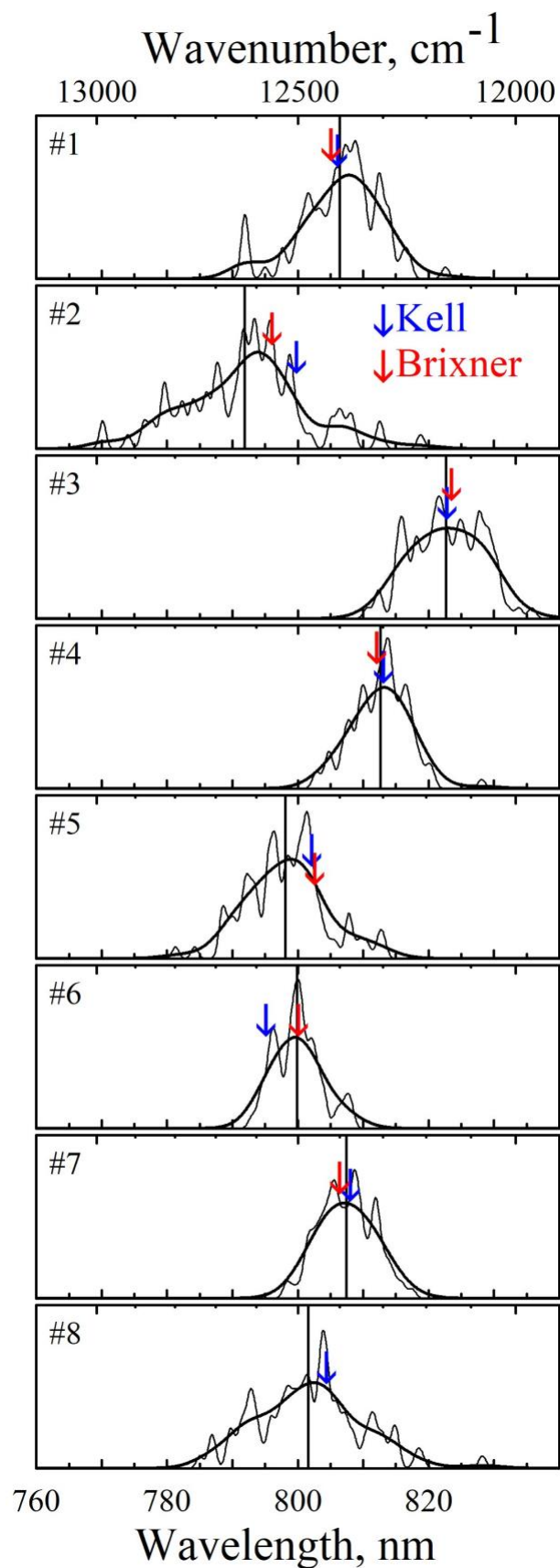


**Figure 3.** QM/EFP site energy fluctuations and comparison to model Hamiltonians by Kell<sup>25</sup> and Brixner<sup>8</sup>. QM/EFP excitation energies are shifted by  $-2430\text{ cm}^{-1}$  to match experimental absorption and CD spectra. Note that the Brixner Hamiltonian contains only seven pigments. QM/EFP site energy stick spectra of 100 snapshots of MD trajectory are broadened by gaussians with FWHM of 20 (thinner black lines) and  $100\text{ cm}^{-1}$  (thicker black lines). Average QM/EFP site energies are shown with black vertical lines; the site energies from Kell and Brixner empirical Hamiltonians are shown with blue and red arrows, respectively.

Average Hamiltonian									Standard Deviation								
QM/EFP	1	2	3	4	5	6	7	8	QM/EFP	1	2	3	4	5	6	7	8
1	14830.4	-113.4	5.3	-6.5	6.4	-8.9	-2.7	24.0	1	94.3	6.4	0.5	0.5	0.6	3.7	1.4	4.5
2	-113.4	15058.8	36.8	9.5	1.6	11.7	6.9	5.7	2	6.4	146.0	1.9	0.8	0.8	1.3	2.0	1.5
3	5.3	36.8	14585.3	-52.0	-2.0	-10.1	7.2	1.4	3	0.5	1.9	79.2	7.4	1.2	0.4	5.0	0.4
4	-6.5	9.5	-52.0	14736.3	-84.0	-19.3	-54.3	-2.0	4	0.5	0.8	7.4	64.8	6.5	1.3	6.6	0.2
5	6.4	1.6	-2.0	-84.0	14959.2	51.2	5.0	4.4	5	0.6	0.8	1.2	6.5	95.4	7.4	3.0	0.3
6	-8.9	11.7	-10.1	-19.3	51.2	14932.0	26.7	-11.2	6	3.7	1.3	0.4	1.3	7.4	54.7	4.3	1.4
7	-2.7	6.9	7.2	-54.3	5.0	26.7	14815.3	-14.1	7	1.4	2.0	5.0	6.6	3.0	4.3	63.3	0.8
8	24.0	5.7	1.4	-2.0	4.4	-11.2	-14.1	14904.9	8	4.5	1.5	0.4	0.2	0.3	1.4	0.8	123.9

**Figure 4.** Averaged QM/EFP Hamiltonian and standard deviations of all matrix elements. All values are in  $\text{cm}^{-1}$ . The 8th pigment is BChl *a* #8' as shown in Figure 1.

Diagonalization of the electronic Hamiltonian produces excitonic states that are visualized and analyzed in Figure S11 of Supporting Information. Overall, an excitonic map of a 7-site model (when BChl *a* #8' is excluded from the Hamiltonian) is in an excellent agreement with that from Brixner's Hamiltonians<sup>8</sup>, while the 8-site model differs from Kell's Hamiltonian<sup>25</sup> in the relative order of pairs of excitons 5 and 6, and 7 and 8.

The excitonic Hamiltonian can be utilized to model absorption (OD) and CD spectra. Detailed comparison of spectra built off on the average electronic Hamiltonian and by averaging the

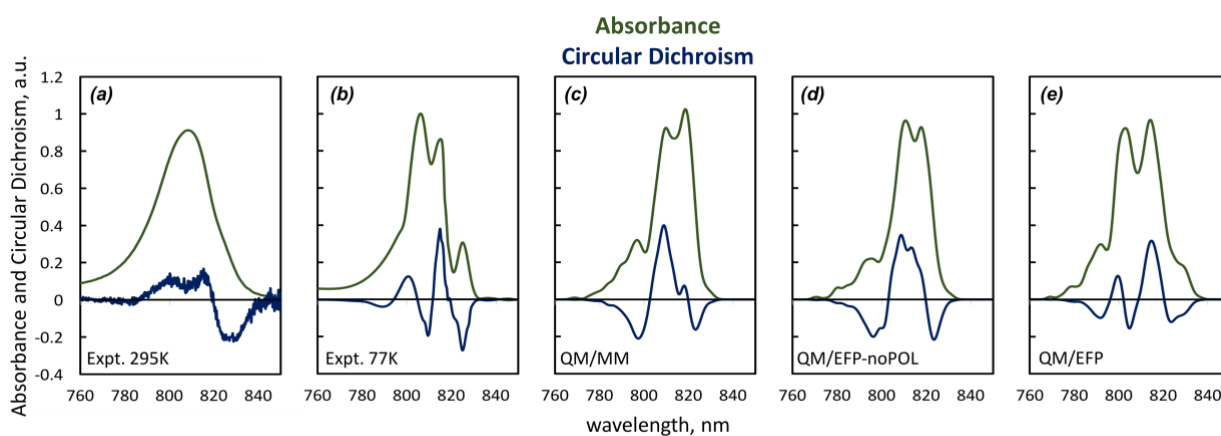


1  
2  
3 spectra of different structural snapshots, as well as comparisons between transition charges and  
4 point dipole approximation models, is provided in Supporting Information (Figures S12, S13,  
5 S14, S15). Here we concentrate on comparing the absorption and CD spectra computed with the  
6 three embedding models, QM/MM, QM/EFP-noPOL, QM/EFP. All spectra are computed as  
7 averages of spectra of individual structural snapshots, i.e. thermal motion of the protein is  
8 directly accounted for. These data are presented in Figure 5, together with experimental  
9 absorption and CD spectra measured at 295 K and 77 K, as further described in Supporting  
10 Information.

11  
12 It is known from experimental studies<sup>65</sup> that BChl *a* #8 is only weakly bound in the FMO  
13 protein and an occupancy of site #8 depends on a protein preparation procedure. It is estimated  
14 that in the procedure utilized in samples that were used for measuring the spectra shown in  
15 Figures 4a and 4b, BChl *a* #8 is present in ~55% of cases.<sup>17, 28</sup> Thus, we mimicked a partial  
16 occupancy of site #8 by combining spectra of individual snapshots with a proportion of 45% of  
17 7-site Hamiltonians and 55% of 8-site Hamiltonians.

18  
19 Analyzing Figure 5, it is noteworthy that the quality of the QM/MM, QM/EFP-noPOL and  
20 QM/EFP models cannot be deduced from comparing absorption spectra alone, as all three  
21 models produce two intense central peaks and red- and blue-side shoulders. However, the  
22 QM/EFP absorption spectrum appears to be somewhat more structured with a more pronounced  
23 red-side shoulder that corresponds to the absorption of the lowest energy excitonic state. CD  
24 spectra provide a more stringent test for the model accuracy, as the signal from different  
25 excitonic transitions can have both positive and negative signs. Out of the three computational  
26 models, only QM/EFP manages to reproduce characteristic (starting from the red side) down-up-  
27 down-up-down sequence of peaks observed both in high and low temperature CD experiments,  
28  
29  
30  
31  
32  
33  
34  
35  
36  
37  
38  
39  
40  
41  
42  
43  
44  
45  
46  
47  
48  
49  
50  
51  
52  
53  
54  
55  
56  
57  
58  
59  
60

1  
2  
3 while the QM/MM and QM/EFP-noPOL models fail to reproduce a qualitative shape of the  
4 experimental CD spectra. A decomposition of the absorption and CD spectra into contributions  
5 of individual excitonic states is provided in Supporting Information (Figures S12 and S13), from  
6 which it follows that the first (right-most, negative) and second (positive) peaks in CD are  
7 produced by the lowest energy excitons 1 and 2, while exciton 4 determines the third (negative)  
8 peak of CD. Interestingly, exciton 3 has opposite (positive or negative) CD signals in 7-site and  
9 8-site models, due to the contribution of BChl *a* #8'. Overall, we conclude that only the  
10 polarizable QM/EFP model faithfully captures excitonic interactions in FMO and is capable of  
11 reproducing quantitatively both absorption and CD spectra.  
12  
13  
14  
15  
16  
17  
18  
19  
20  
21  
22  
23  
24  
25  
26



27  
28  
29  
30  
31  
32  
33  
34  
35  
36  
37  
38  
39  
40  
41  
42 **Figure 5.** Absorption (green) and CD (blue) spectra of the FMO complex. Experimental spectra  
43 measured at 295 K (a) and 77 K (b) and computed spectra using QM/MM (c), QM/EFP-noPOL  
44 (d) and QM/EFP (e) models. Computed spectra are obtained by combining spectra of individual  
45 snapshots with a proportion of 45% of 7-site Hamiltonians and 55% of 8-site Hamiltonians. For a  
46 comparison with experimental spectra, QM/MM and QM/EFP-noPOL spectra are shifted by -  
47 2800  $\text{cm}^{-1}$  and QM/EFP spectra are shifted by -2430  $\text{cm}^{-1}$ .  
48  
49  
50  
51  
52  
53  
54  
55  
56  
57  
58  
59  
60

1  
2  
3 We note in passing that the spectra modeled using electronic couplings computed with  
4 transition charges and point dipole approximation are qualitatively similar, with the transition  
5 charge model producing a better-resolved lowest-energy (first exciton) shoulder in the absorption  
6 spectrum and a better-resolved middle region (795-805 nm) of the CD spectrum. Detailed  
7 comparisons of transition charges and point dipole approximation models are provided in  
8 Supporting Information (Figs. S9, S11, S15).  
9  
10  
11  
12  
13  
14  
15  
16  
17

18 To summarize, we developed a multi-scale modeling strategy for describing excitonic  
19 properties of pigment-protein complexes. The modeling is based solely on the x-ray structure of  
20 the protein complex and does not use other input from experiments. The main steps of the  
21 modeling procedure include classical MD simulations, followed by partial correction of pigment  
22 structures by constrained QM/MM geometry optimizations. Then the excited state calculations of  
23 electronic states and transition charges of chromophores are conducted with TD-DFT PBE0/6-  
24 31G(d) in polarizable embedding in which the protein is modeled with the Effective Fragment  
25 Potentials. This computational protocol was successfully applied to model the excitonic  
26 properties of the Fenna-Matthews-Olson photosynthetic complex and resulted in the electronic  
27 Hamiltonian that is in an excellent quantitative agreement with previously proposed empirical  
28 Hamiltonians. The theory reproduces all major features of absorption and CD spectra of the  
29 FMO protein complex. We demonstrate that such an agreement between modeling and  
30 experiment becomes possible due to (i) utilizing accurate structures of photosynthetic pigments  
31 for computing excitation energies, and (ii) representing the protein environment with a  
32 polarizable model. Successful first principles-based modeling of the FMO complex opens  
33 exciting avenues for predictive modeling of other wild type and mutated photosynthetic pigment-  
34  
35  
36  
37  
38  
39  
40  
41  
42  
43  
44  
45  
46  
47  
48  
49  
50  
51  
52  
53  
54  
55  
56  
57  
58  
59  
60

1  
2  
3 protein complexes that will provide mechanistic understanding of interactions in these complex  
4  
5 systems.  
6  
7

8 **Supporting Information.** Supporting Information includes description of experimental methods  
9  
10 and computational details.  
11  
12  
13  
14  
15

## 16 **ACKNOWLEDGMENT**

17  
18  
19 Authors thank Prof. Gerrit Groenhof for sharing topology of BChl force fields. Y.K. and  
20  
21 L.V.S. gratefully acknowledge support from the National Science Foundation (grant CHE-  
22  
23 1800505). S.S., V.S. and L.V.S. acknowledge support from the Department of Energy, office of  
24  
25 Basic Energy Sciences (grant DE-SC0018239). DM acknowledges support from the Academy of  
26  
27 Finland (grant 285481) and also thank the CSC-IT Center for Science in Espoo, Finland, for  
28  
29 providing computational resources. This research was also supported in part through  
30  
31 computational resources provided by Information Technology at Purdue, West Lafayette,  
32  
33  
34  
35  
36 Indiana.  
37  
38  
39  
40  
41

## 42 **References**

- 43  
44  
45 1. Orf, G. S.; Blankenship, R. E., Chlorosome antenna complexes from green  
46  
47 photosynthetic bacteria. *Photosynth. Res.* **2013**, *116* (2), 315-331.  
48 2. Savikhin, S.; Struve, W. S., Ultrafast energy transfer in FMO trimers from the green  
49  
50 bacterium *Chlorobium tepidum*. *Biochemistry* **1994**, *33*, 11200-11208.  
51 3. Savikhin, S.; Struve, W. S., Low-temperature energy transfer in FMO trimers from the  
52  
53 green photosynthetic bacterium *Chlorobium tepidum*. *Photosynth. Res.* **1996**, *48*, 271-276.  
54 4. Buck, D. R.; Savikhin, S.; Struve, W. S., Ultrafast absorption difference spectra of the  
55  
56 FMO protein at 19 K: Experiment and simulations. *Biophys. J.* **1997**, *72*, 24-36.  
57  
58  
59  
60

- 1
  - 2
  - 3
  - 4
  - 5
  - 6
  - 7
  - 8
  - 9
  - 10
  - 11
  - 12
  - 13
  - 14
  - 15
  - 16
  - 17
  - 18
  - 19
  - 20
  - 21
  - 22
  - 23
  - 24
  - 25
  - 26
  - 27
  - 28
  - 29
  - 30
  - 31
  - 32
  - 33
  - 34
  - 35
  - 36
  - 37
  - 38
  - 39
  - 40
  - 41
  - 42
  - 43
  - 44
  - 45
  - 46
  - 47
  - 48
  - 49
  - 50
  - 51
  - 52
  - 53
  - 54
  - 55
  - 56
  - 57
  - 58
  - 59
  - 60
5. Louwe, R. J. W.; Vrieze, J.; Hoff, A. J.; Aartsma, T. J., Toward an integral interpretation of the optical steady-state spectra of the FMO-complex of *Prosthecochloris aestuarii*. 2. Exciton simulations. *J. Phys. Chem. B* **1997**, *101* (51), 11280-11287.
6. Vulto, S. I. E.; de Baat, M. A.; Louwe, R. J. W.; Permentier, H. P.; Neef, T.; Miller, M.; van Amerongen, H.; Aartsma, T. J., Exciton simulations of optical spectra of the FMO complex from the green sulfur bacterium *Chlorobium tepidum* at 6 K. *J. Phys. Chem. B* **1998**, *102* (47), 9577-9582.
7. Vulto, S. I. E.; de Baat, M. A.; Neerken, S.; Nowak, F. R.; van Amerongen, H.; Amesz, J.; Aartsma, T. J., Excited state dynamics in FMO antenna complexes from photosynthetic green sulfur bacteria: a kinetic model. *J. Phys. Chem. B* **1999**, *103* (38), 8153-8161.
8. Brixner, T.; Stenger, J.; Vaswani, H. M.; Cho, M.; Blankenship, R. E.; Fleming, G. R., Two-dimensional spectroscopy of electronic couplings in photosynthesis. *Nature* **2005**, *434* (7033), 625-628.
9. Olson, J., The FMO protein. In *Discoveries in Photosynthesis*, Govindjee; Beatty, J. T.; Gest, H.; Allen, J., Eds. Springer Netherlands: 2005; Vol. 20, pp 421-427.
10. Adolphs, J.; Muh, F.; Madjet, M. E. A.; Renger, T., Calculation of pigment transition energies in the FMO protein. *Photosynth. Res.* **2008**, *95* (2-3), 197-209.
11. Tronrud, D. E.; Wen, J. Z.; Gay, L.; Blankenship, R. E., The structural basis for the difference in absorbance spectra for the FMO antenna protein from various green sulfur bacteria. *Photosynth. Res.* **2009**, *100* (2), 79-87.
12. Milder, M. T. W.; Bruggemann, B.; van Grondelle, R.; Herek, J. L., Revisiting the optical properties of the FMO protein. *Photosynth. Res.* **2010**, *104* (2-3), 257-274.
13. Moix, J.; Wu, J.; Huo, P.; Coker, D.; Cao, J., Efficient Energy Transfer in Light-Harvesting Systems, III: The Influence of the Eighth Bacteriochlorophyll on the Dynamics and Efficiency in FMO. *J. Phys. Chem. Lett.* **2011**, *2* (24), 3045-3052.
14. Olbrich, C.; Jansen, T. L. C.; Liebers, J.; Aghtar, M.; Strumpf, J.; Schulten, K.; Knoester, J.; Kleinekathofer, U., From Atomistic Modeling to Excitation Transfer and Two-Dimensional Spectra of the FMO Light-Harvesting Complex. *J. Phys. Chem. B* **2011**, *115* (26), 8609-8621.
15. Olbrich, C.; Strumpf, J.; Schulten, K.; Kleinekathofer, U., Quest for Spatially Correlated Fluctuations in the FMO Light-Harvesting Complex. *J. Phys. Chem. B* **2011**, *115* (4), 758-764.
16. Schmidt am Busch, M.; Müh, F.; El-Amine Madjet, M.; Renger, T., The Eighth Bacteriochlorophyll Completes the Excitation Energy Funnel in the FMO Protein. *J. Phys. Chem. Lett.* **2011**, *2* (2), 93-98.
17. Wen, J.; Zhang, H.; Gross, M. L.; Blankenship, R. E., Native Electrospray Mass Spectrometry Reveals the Nature and Stoichiometry of Pigments in the FMO Photosynthetic Antenna Protein. *Biochemistry* **2011**, *50* (17), 3502-3511.
18. Fidler, A. F.; Caram, J. R.; Hayes, D.; Engel, G. S., Towards a coherent picture of excitonic coherence in the Fenna-Matthews-Olson complex. *J. Phys. B: At. Mol. Opt. Phys.* **2012**, *45* (15).
19. Gao, J. K.; Shi, W. J.; Ye, J.; Wang, X. Q.; Hirao, H.; Zhao, Y., QM/MM Modeling of Environmental Effects on Electronic Transitions of the FMO Complex. *J. Phys. Chem. B* **2013**, *117* (13), 3488-3495.

- 1  
2  
3 20. List, N. H.; Curutchet, C.; Knecht, S.; Mennucci, B.; Kongsted, J., Toward Reliable  
4 Prediction of the Energy Ladder in Multichromophoric Systems: A Benchmark Study on the  
5 FMO Light-Harvesting Complex. *J. Chem. Theory Comput.* **2013**, *9* (11), 4928-4938.
- 6 21. Jurinovich, S.; Curutchet, C.; Mennucci, B., The Fenna-Matthews-Olson Protein  
7 Revisited: A Fully Polarizable (TD)DFT/MM Description. *ChemPhysChem* **2014**, *15* (15), 3194-  
8 3204.
- 9 22. Chandrasekaran, S.; Aghtar, M.; Valleau, S.; Aspuru-Guzik, A.; Kleinekathöfer, U.,  
10 Influence of Force Fields and Quantum Chemistry Approach on Spectral Densities of BChl a in  
11 Solution and in FMO Proteins. *J. Phys. Chem. B* **2015**, *119* (31), 9995-10004.
- 12 23. Jia, X. Y.; Mei, Y.; Zhang, J. Z. H.; Mo, Y., Hybrid QM/MM study of FMO complex  
13 with polarized protein-specific charge. *Sci. Rep.* **2015**, *5*, 17096.
- 14 24. Higashi, M.; Saito, S., Quantitative Evaluation of Site Energies and Their Fluctuations of  
15 Pigments in the Fenna-Matthews-Olson Complex with an Efficient Method for Generating a  
16 Potential Energy Surface. *J. Chem. Theory Comput.* **2016**, *12* (8), 4128-4137.
- 17 25. Kell, A.; Blankenship, R. E.; Jankowiak, R., Effect of Spectral Density Shapes on the  
18 Excitonic Structure and Dynamics of the Fenna-Matthews-Olson Trimer from *Chlorobaculum*  
19 *tepidum*. *J. Phys. Chem. A* **2016**, *120* (31), 6146-6154.
- 20 26. Schulze, J.; Shibl, M. F.; Al-Marri, M. J.; Kühn, O., Multi-layer multi-configuration  
21 time-dependent Hartree (ML-MCTDH) approach to the correlated exciton-vibrational dynamics  
22 in the FMO complex. *J. Chem. Phys.* **2016**, *144* (18), 185101.
- 23 27. Padula, D.; Lee, M. H.; Claridge, K.; Troisi, A., Chromophore-Dependent Intramolecular  
24 Exciton-Vibrational Coupling in the FMO Complex: Quantification and Importance for Exciton  
25 Dynamics. *J. Phys. Chem. B* **2017**, *121* (43), 10026-10035.
- 26 28. Saer, R. G.; Stadnytskyi, V.; Magdaong, N. C.; Goodson, C.; Savikhin, S.; Blankenship,  
27 R. E., Probing the excitonic landscape of the *Chlorobaculum tepidum* Fenna-Matthews-Olson  
28 (FMO) complex: a mutagenesis approach. *Biochimica et Biophysica Acta (BBA) - Bioenergetics*  
29 **2017**, *1858* (4), 288-296.
- 30 29. Kim, C. W.; Choi, B.; Rhee, Y. M., Excited state energy fluctuations in the Fenna-  
31 Matthews-Olson complex from molecular dynamics simulations with interpolated chromophore  
32 potentials. *Phys. Chem. Chem. Phys.* **2018**, *20* (5), 3310-3319.
- 33 30. Matthews, B. W.; Fenna, R. E.; Bolognesi, M. C.; Schmid, M. F.; Olson, J. M., Structure  
34 of a bacteriochlorophyll *a*-protein from the green photosynthetic bacterium *Prosthecochloris*  
35 *aestuarii*. *J. Mol. Biol.* **1979**, *131* (2), 259-285.
- 36 31. Buck, D. R.; Savikhin, S.; Struve, W. S., Effect of diagonal energy disorder on circular  
37 dichroism spectra of Fenna-Matthews-Olson trimers. *J. Phys. Chem. B* **1997**, *101* (42), 8395-  
38 8397.
- 39 32. Savikhin, S.; Buck, D. R.; Struve, W. S., Toward level-to-level energy transfers in  
40 photosynthesis: the Fenna-Matthews-Olson protein. *J. Phys. Chem. B* **1998**, *102*, 5556-5565.
- 41 33. Savikhin, S.; Buck, D. R.; Struve, W. S., The Fenna-Matthews-Olson protein: a strongly  
42 coupled photosynthetic antenna. In *Resonance energy transfer*, Andrews, D. L.; Demidov, A. A.,  
43 Eds. John Wiley & Sons: New York, 1999; pp 399-434.
- 44 34. Kihara, S.; Hartzler, D.; Orf, G. S.; Blankenship, R. E.; Savikhin, S., The Fate of the  
45 Triplet Excitations in the Fenna-Matthews-Olson Complex and Stability of the Complex.  
46 *Biophys. J.* **2014**, *106* (2, Supplement 1), 182a.
- 47 35. Saito, S.; Higashi, M.; Fleming, G. R., Site-Dependent Fluctuations Optimize Electronic  
48 Energy Transfer in the Fenna-Matthews-Olson Protein. *J. Phys. Chem. B* **2019**.
- 49  
50  
51  
52  
53  
54  
55  
56  
57  
58  
59  
60

- 1  
2  
3 36. Khmel'nitskiy, A.; Reinot, T.; Jankowiak, R., Impact of Single-Point Mutations on the  
4 Excitonic Structure and Dynamics in a Fenna–Matthews–Olson Complex. *J. Phys. Chem. Lett.*  
5 **2018**, *9* (12), 3378-3386.
- 6 37. Fransted, K. A.; Caram, J. R.; Hayes, D.; Engel, G. S., Two-dimensional electronic  
7 spectroscopy of bacteriochlorophyll a in solution: Elucidating the coherence dynamics of the  
8 Fenna-Matthews-Olson complex using its chromophore as a control. *J. Chem. Phys.* **2012**, *137*  
9 (12), 125101.
- 10 38. Savikhin, S.; Buck, D. R.; Struve, W. S., Oscillating anisotropies in a bacteriochlorophyll  
11 protein: evidence for quantum beating between exciton levels. *Chem. Phys.* **1997**, *223*, 303-312.
- 12 39. Allodi, M. A.; Otto, J. P.; Sohail, S. H.; Saer, R. G.; Wood, R. E.; Rolczynski, B. S.;  
13 Massey, S. C.; Ting, P.-C.; Blankenship, R. E.; Engel, G. S., Redox Conditions Affect Ultrafast  
14 Exciton Transport in Photosynthetic Pigment–Protein Complexes. *The Journal of Physical*  
15 *Chemistry Letters* **2018**, *9* (1), 89-95.
- 16 40. Fidler, A. F.; Caram, J. R.; Hayes, D.; Engel, G. S., Towards a coherent picture of  
17 excitonic coherence in the Fenna–Matthews–Olson complex. *Journal of Physics B: Atomic,*  
18 *Molecular and Optical Physics* **2012**, *45* (15), 154013.
- 19 41. Engel, G. S., Quantum coherence in photosynthesis. *Procedia Chemistry* **2011**, *3* (1),  
20 222-231.
- 21 42. Curutchet, C.; Mennucci, B., Quantum Chemical Studies of Light Harvesting. *Chem.*  
22 *Rev. (Washington, DC, U. S.)* **2017**, *117* (2), 294-343.
- 23 43. Groenhof, G.; Modi, V.; Morozov, D., Observe while it happens: catching photoactive  
24 proteins in the act with non-adiabatic molecular dynamics simulations. *Curr. Opin. Struct. Biol.*  
25 **2020**, *61*, 106-112.
- 26 44. Kaliakin, D. S.; Nakata, H.; Kim, Y.; Chen, Q.; Fedorov, D. G.; Slipchenko, L. V.,  
27 FMOx FMO: Elucidating Excitonic Interactions in the Fenna–Matthews–Olson Complex with the  
28 Fragment Molecular Orbital Method. *J. Chem. Theory Comput.* **2019** DOI:  
29 10.1021/acs.jctc.9b00621.
- 30 45. Kosenkov, D.; Slipchenko, L. V., Solvent effects on the electronic transitions of p-  
31 nitroaniline: A QM/EFP study. *J. Phys. Chem. A* **2010**, *115* (4), 392-401.
- 32 46. Ghosh, D.; Isayev, O.; Slipchenko, L. V.; Krylov, A. I., Effect of solvation on the vertical  
33 ionization energy of thymine: from microhydration to bulk. *J. Phys. Chem. A* **2011**, *115* (23),  
34 6028-6038.
- 35 47. Slipchenko, L. V., Solvation of the Excited States of Chromophores in Polarizable  
36 Environment: Orbital Relaxation versus Polarization. *J. Phys. Chem. A* **2010**, *114* (33), 8824-  
37 8830.
- 38 48. DeFusco, A.; Minezawa, N.; Slipchenko, L. V.; Zahariev, F.; Gordon, M. S., Modeling  
39 Solvent Effects on Electronic Excited States. *J. Phys. Chem. Lett.* **2011**, *2* (17), 2184-2192.
- 40 49. Gordon, M. S.; Smith, Q. A.; Xu, P.; Slipchenko, L. V., Accurate First Principles Model  
41 Potentials for Intermolecular Interactions. *Annu. Rev. Phys. Chem.* **2013**, *64*, 553-578.
- 42 50. Gurunathan, P. K.; Acharya, A.; Ghosh, D.; Kosenkov, D.; Kaliman, I.; Shao, Y. H.;  
43 Krylov, A. I.; Slipchenko, L. V., Extension of the Effective Fragment Potential Method to  
44 Macromolecules. *J. Phys. Chem. B* **2016**, *120* (27), 6562-6574.
- 45 51. Slipchenko, L. V.; Gurunathan, P. K., Effective Fragment Potential Method: Past,  
46 Present, and Future. In *Fragmentation: Toward Accurate Calculations on Complex Molecular*  
47 *Systems*, Gordon, M. S., Ed. Wiley: 2017; pp 183-208.
- 48  
49  
50  
51  
52  
53  
54  
55  
56  
57  
58  
59  
60

- 1  
2  
3 52. Day, P. N.; Jensen, J. H.; Gordon, M. S.; Webb, S. P.; Stevens, W. J.; Krauss, M.;  
4 Garmer, D.; Basch, H.; Cohen, D., An effective fragment method for modeling solvent effects in  
5 quantum mechanical calculations. *J. Chem. Phys.* **1996**, *105* (5), 1968-1986.
- 6 53. Gordon, M. S.; Freitag, M. A.; Bandyopadhyay, P.; Jensen, J. H.; Kairys, V.; Stevens, W.  
7 J., The effective fragment potential method: A QM-based MM approach to modeling  
8 environmental effects in chemistry. *J. Phys. Chem. A* **2001**, *105* (2), 293-307.
- 9 54. Gordon, M. S.; Slipchenko, L.; Li, H.; Jensen, J. H., Chapter 10 The Effective Fragment  
10 Potential: A General Method for Predicting Intermolecular Interactions. In *Annual Reports in*  
11 *Computational Chemistry*, Spellmeyer, D. C.; Wheeler, R., Eds. Elsevier: 2007; Vol. 3, pp 177-  
12 193.
- 13 55. Kaliman, I. A.; Slipchenko, L. V., LIBEFP: A new parallel implementation of the  
14 effective fragment potential method as a portable software library. *J. Comput. Chem.* **2013**, *34*  
15 (26), 2284-2292.
- 16 56. Kaliman, I. A.; Slipchenko, L. V., Hybrid MPI/OpenMP Parallelization of the Effective  
17 Fragment Potential Method in the libefp Software Library. *J. Comput. Chem.* **2015**, *36* (2), 129-  
18 135.
- 19 57. Ghosh, D.; Kosenkov, D.; Vanovschi, V.; Williams, C. F.; Herbert, J. M.; Gordon, M. S.;  
20 Schmidt, M. W.; Slipchenko, L. V.; Krylov, A. I., Noncovalent interactions in extended systems  
21 described by the effective fragment potential method: Theory and application to nucleobase  
22 oligomers. *J. Phys. Chem. A* **2010**, *114* (48), 12739-12754.
- 23 58. Slipchenko, L. V., Effective Fragment Potential Method. In *Many-Body Effects and*  
24 *Electrostatics in Biomolecules*, Cui, Q.; Meuwly, M.; Ren, P., Eds. CRC Press: 2016; pp 147-  
25 190.
- 26 59. Gordon, M. S.; Fedorov, D. G.; Pruitt, S. R.; Slipchenko, L. V., Fragmentation methods:  
27 a route to accurate calculations on large systems. *Chem. Rev. (Washington, DC, U. S.)* **2011**, *112*  
28 (1), 632-672.
- 29 60. Gordon, M. S.; Fedorov, D. G.; Pruitt, S. R.; Slipchenko, L. V., Fragmentation Methods:  
30 A Route to Accurate Calculations on Large Systems. *Chem. Rev. (Washington, DC, U. S.)* **2012**,  
31 *112* (1), 632-672.
- 32 61. Sisto, A.; Glowacki, D. R.; Martinez, T. J., Ab Initio Nonadiabatic Dynamics of  
33 Multichromophore Complexes: A Scalable Graphical-Processing-Unit-Accelerated Exciton  
34 Framework. *Acc. Chem. Res.* **2014**, *47* (9), 2857-2866.
- 35 62. Segatta, F.; Cupellini, L.; Garavelli, M.; Mennucci, B., Quantum Chemical Modeling of  
36 the Photoinduced Activity of Multichromophoric Biosystems. *Chem. Rev. (Washington, DC, U.*  
37 *S.)* **2019**, *119* (16), 9361-9380.
- 38 63. Curutchet, C.; Kongsted, J.; Muñoz-Losa, A.; Hossein-Nejad, H.; Scholes, G. D.;  
39 Mennucci, B., Photosynthetic Light-Harvesting Is Tuned by the Heterogeneous Polarizable  
40 Environment of the Protein. *J. Am. Chem. Soc.* **2011**, *133* (9), 3078-3084.
- 41 64. Aghtar, M.; Kleinekathöfer, U.; Curutchet, C.; Mennucci, B., Impact of Electronic  
42 Fluctuations and Their Description on the Exciton Dynamics in the Light-Harvesting Complex  
43 PE545. *J. Phys. Chem. B* **2017**, *121* (6), 1330-1339.
- 44 65. Ben-Shem, A.; Frolow, F.; Nelson, N., Evolution of photosystem I – from symmetry  
45 through pseudosymmetry to asymmetry. *FEBS Lett.* **2004**, *564* (3), 274-280.
- 46  
47  
48  
49  
50  
51  
52  
53  
54  
55  
56  
57  
58  
59  
60